Optical self-organization and cavity solitons in optically pumped semiconductor microresonators

Y. Menesguen, S. Barbay, X. Hachair, L. Leroy, I. Sagnes, and R. Kuszelewicz*
Laboratoire de Photonique et Nanostructures, route de Nozay 91460 Marcoussis, France
(Received 13 March 2006; published 29 August 2006)

We study the self-organizing properties of an optically driven semiconductor microresonator especially designed and optimized for optical pumping wherein patterns and cavity solitons are observed for the first time with all-optical excitations. We demonstrate both coherent and incoherent writing and erasure of cavity solitons achievable on the same sample, enriching the spectrum of the system functionalities. Finally, we show how the system lends itself to the multiplication of the number of cavity solitons and how they possibly coexist.

DOI: 10.1103/PhysRevA.74.023818 PACS number(s): 42.65.Tg, 42.65.Sf, 68.65.−k

I. INTRODUCTION

Cavity solitons (CSs) have the twofold characteristic of being exotic, self-organized states emerging from light-matter interaction within a nonlinear microresonator and that of appearing as promising candidates for the structuration, the manipulation, and the plastic transformation of two-dimensional (2D) binary optical information. CSs are self-localized spots forming in the transverse plane of spatially extended, bistable, and modulationally unstable cavities or feedback mirror systems, and generally appear as bright spots sitting on a dark background. CSs can be independently addressed with a control beam and can be manipulated with phase or amplitude gradients of the injected field [1]. As such, they can be thought of as logical binary units for parallel information processing with reconfiguration capabilities. Their observation in various macroscopic materials [2–5] and more recently their first prediction [6], and their demonstration in microscopic semiconductor structures [7] bring the important confirmation that they have the capability to produce novel and efficient functional concepts that can renew the field of all-optical information processing. In this respect, the application of such concepts to semiconductor materials has proved particularly challenging, thanks to the time (<1 ns) and spatial scales (~ 10 μm) they involve. They have been studied in integrated microresonators, mostly in the form of vertical cavity surface emitting lasers (VCSELs).

Among relevant systems for CS formation are those that contain passive materials, preferably exhibiting either a focusing nonlinearity or a saturable absorption. Such systems have been quite successful in the form of atomic vapors or liquid crystal light valves, but they have the disadvantage of being slow and inappropriate for miniaturization and integration. However, although patterns could be found [8,9] in passive semiconductors, CS demonstration failed due to the defocusing character of the dispersive nonlinearity in the vicinity of direct gap III-V compounds [10]. However, focusing nonlinearities can be sought in quantum dot semiconductor layers, as was predicted in a recent theoretical work [11,12], and their versatile properties open quite promising perspectives. Another approach followed experimentally consists of addressing active systems by exciting III-V semiconductors above transparency by means of an external injection of carriers. This is equivalent to tailoring the material susceptibility, hence producing gain and eventually a focusing nonlinearity.

The first demonstration of CSs in semiconductors, reported in [7], used an electrically pumped 150 μm diameter vertical cavity semiconductor optical amplifier (VCSOA) optically injected by a coherent beam, the holding beam (HB). This revealed rather stringent requirements on the transverse distribution of the excitation due to the generally high sensitivity of CS on the transverse uniformity of external parameters. By contrast, optical pumping certainly introduces an improved control of the transverse homogeneity, thanks to the current availability of fiber coupled high power laser diodes, though it requires design and engineering procedures to optimize the coupling between the pump beam and the nonlinear material [13]. With this revisited approach of resonator and cavity operation, CSs are expected to be more predictably found and easier to manipulate. In this respect, writing and erasure of CSs represent a first step in the manipulation of optical bits of information [14]. Switching of spatial localized structures has been discussed by several authors. Solitons have been actually written and erased in VCSOA electrically pumped below threshold and injected with a coherent excitation [7,15], and their dynamics is analyzed in [16]. The situations described therein correspond to what in this paper will be termed coherent writing and erasure, since the writing or erasure fields need to have a defined phase relation with the HB. Many applications can be conceived in this context of coherent fields. As predicted by [17], the process of incoherent switching of CSs is complementary in terms of functionalities, and to our best knowledge it had been demonstrated only quite recently [18]. In this context, the writing and/or erasure pulses proceed by a direct generation of carriers. Incoherent switching has also been used in [19], where a writing beam with a polarization perpendicular to that of the HB was shown to switch a bistable structure in a passive semiconductor system. In that case, spatial decorrelation was not shown across the cavity and only a single spatial structure could be manipulated. In addition, the very high level of intensity sent onto the sample, which was not provided with any heat dissipating system, brought in a strong thermal component in the dynamics that excludes an intrepretation in terms of cavity solitons, as was shown sub-

*Electronic address: robert.kuszelewicz@lpn.cnrs.fr; URL: http://www.lpn.cnrs.fr/

sequently in [10]. An optically pumped microresonator has also been studied in[20]. In this case, the working diameter of the Gaussian HB, of the order of 50 μm, strongly correlated the observed localized state to the boundary conditions. Switching of the localized structure has been probed by ramping the whole HB or pump beam, but the manipulation with an external writing beam has not been reported. In that case, the arguments developed in [10] and related to thermal dissipation still hold.

In the present paper, we report on the study and the observation of a series of self-organized states resulting from light-matter interaction in an optically pumped GaAs-based microresonator. These results were obtained by realizing microresonators optimized for a maximum optical injection efficiency, including *ab initio* considerations for thermal management. These aspects are developed in Sec. II. In Sec. III we describe the experimental characterization steps that we performed in order to fully quantify the actual performance of optimized resonators, and in Sec. IV we describe the first achievements of self-organized states in above transparency optically pumped VCSOA. In the Sec. V the incoherent and coherent writing and erasure processes of the CS are reported. Finally, some more complex states of the microresonator optical response, displaying multiple CSs, are presented in Sec. VI, before the Conclusion.

II. OPTIMIZATION, DESIGN, AND REALIZATION OF MICRORESONATORS

Our samples are based on a specific design following a procedure described in [13]. We use an optically pumped VSCOA in the AlGaAs material system. Optical pumping is used in order to improve the uniformity of the pumped region, by contrast with an electrically pumped VCSEL. In the latter type of injection, due to an aluminum oxide diaphragm, the current crowding effect introduces an excess carrier injection at the edges of the microcavity and brings the peripheral part of the excited region at threshold first. Another cause of departure from uniformity is the annular geometry of the electrodes which produces a depression in the center of the current distribution. This has been controlled to a certain extent by the use of bottom emitting VCSEL [21], which proved very efficient up to 100–200 μm diameter. However, in the context of electrical injection, a further increase of the diameters should call for different technologies, such as indium-titanium oxide or gridded contacts. On the contrary, an actually available fibered diode laser provided extremely flat optical pumping sources with diameters larger than 1 mm.

With optical pumping, we expect in addition a reduction in the heat production, since there are no heat sources in the mirrors and the system is intrinsically free from the Joule effect. Our design procedure incorporates the calculation of thermal dissipation, following the mathematical approach developed in [22]. With the improvement of thermal management, scalability can be envisioned by pushing up excited cross section diameters toward the millimeter scale. One of the most important assets of optical pumping is the flexibility introduced in the choice of the sample region to be studied. More generally, calling for external beams for structuring the material properties is a quite versatile and reversible approach. This argument is not only valid for the pump beam, at the present exploratory stage of this study, but can also be invoked as a mean for introducing reconfiguration properties in highly parallel optical processing schemes [23]. Finally, the reduced number of technological steps required to reach the final sample is likely to limit the occurrence of localized defects in the material structure that may cause cavity soliton pinning.

The cavity is composed of two aperiodic AlAs/AlGaAs multilayer mirrors designed for an optimal optical pumping efficiency at 800 nm. These mirrors are calculated with a special optimization procedure such that a pump window is created on the high-energy side of the mirror stop band to allow optical pumping over a 20 nm spectral width with a maximum pump absorption. At the same time, we require that the pump intensity not absorbed in the active zone be reflected by the back mirror in order to prevent absorption by the substrate. The active zone is composed of a bulk GaAs layer surrounded by two $Al_{0.07}Ga_{0.93}As$ absorbing spacers. We built an error function that measures the distance between the targeted properties and those calculated, given the set of layer widths composing the stack. This function takes the individual properties of each mirror (reflection, phase in reflection) into account along with the absorption of the complete cavity filled by the active medium, each with a given weight. A standard simplex algorithm is then used to find the minimum of the error function with respect to the thicknesses of the layers composing the stack. The optimization is complete when a local minimum of the function has been found and when a satisfying solution is reached.

The resonator is first grown upside-down by metal-organic chemical vapor deposition. The sample is then bonded onto a SiC substrate using a $AuIn_2$ layer. After etching away the GaAs substrate, we finally obtain a resonator with optimized pumping and heat dissipation, which are crucial requirements if one wishes to pump large diameter cavities [22]. The sample has a cavity resonance gradient in the transverse plane due to the growth conditions estimated around 40 GHz/100 μm, i.e., 0.8 Å/100 μm. This gradient has a negligible effect on the optical response in comparison with gradients of other origins (thermal gradients, thickness fluctuations, spatial defects). The laser threshold is crossed for a pump intensity of $\sim$38 kW/cm^2 and a 70 μm pump diameter, which is consistent with standard GaAs material parameters and mirror reflectivities of 0.986 and 0.995, respectively, for the front and back mirrors. For a 120 μm pump diameter, the threshold was never reached for the powers available in our experiment.

III. EXPERIMENTAL SETUP AND CONFIGURATIONS

In addition to the HB and, in some experiments, to a WB needed to drive the cavity, our experimental setup must also handle an optical pump beam (PB). All beams must be focused onto the sample. The experimental setup is sketched in Fig. 1. It encompasses various possible configurations that are used sequentially in Secs. IV and V.

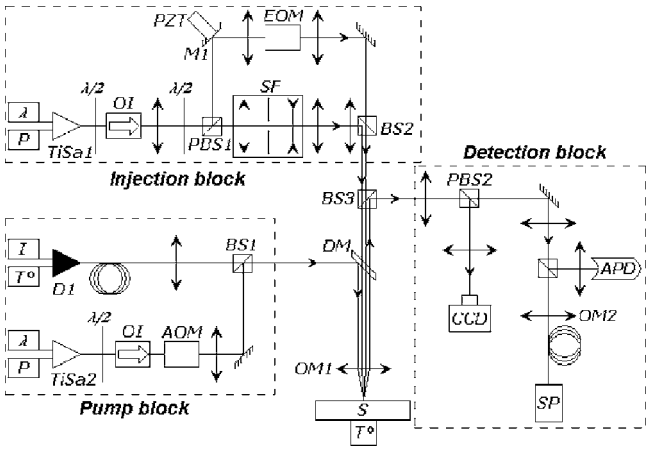

FIG. 1. Experimental setup. D1, high power fiber-coupled diode laser array; TiSa1, tunable Ti:Sapphire ring cavity laser; OI, optical isolator; PBS1, PBS2, polarized beamsplitters; BS1, BS2, BS3, beamsplitters; SF, beam expander with spatial filtering; EOM, electro-optic modulator; PZT, piezoelectric holder; M1, mirror; AOM, acousto-optic modulator; DM, dichroic mirror; OM1, microscope objective (×20 or ×40); S, sample mounted on a Peltier cooler; CCD, CCD camera; APD, avalanche photodiode; and SP, spectrometer.

The setup is composed of three different blocks. Two of them provide light sources each of specific wavelengths, and the third block is dedicated to detection and analysis. The two source blocks have the same internal structure: one arm is the continuous wave (cw) or slowly modulated beam, while an additional arm provides transient perturbations at the same wavelength. The pump block is composed of a fiber coupled high power cw laser diode array operating at around 800 nm, which can deliver up to 12 W. The linewidth is 1.5 nm, and the numerical aperture of the 800 μm core diameter fiber is 0.18. This beam is directed onto the sample through the dichroic mirror (DM). Thus, when focused on the sample, the pump beam provides a uniform pump intensity of up to several tens of kW cm^{-2} on a surface ranging from 70 μm to 200 μm diameter, depending on the microscope objective OM1 used. Transient pulses are produced by a second Ti:sapphire ring cavity laser (TiSa2) which can run around 795 nm either in the cw regime or in the mode-locked (ML) regime.

The injection block provides coherent light beams for injection. The HB which drives the field into the cavity is produced by a tunable Ti:sapphire ring cavity laser (TiSa1) whose output wavelength can be precisely tuned from less than 800 nm to more than 900 nm thanks to intracavity etalons. The HB is then cleaned via a spatial filter (SF) in the Fourier space. In order to broaden the waist of the HB on the sample to a diameter larger than that of the pumped region, a telescope is introduced in its path.

Depending on the precise experiment we undertook, either the PB or the HB is combined with a WB whose shaping details are described in Sec. IV. The PB, the HB, and eventually the WB are combined with DM, which is a key element of the setup first combining then separating the beams of different wavelengths issued from each source block.

The sample is mounted on a Peltier cooler and its temperature is controlled by a feedback loop with a stability of about 10^{-2} K close to 275 K. The output of the VCSOA is studied in reflectivity within the detection and analysis block. The near field is reimaged on a charge-coupled device (CCD) camera and on a fast avalanche photodiode (APD), with 90 ps rise time for local dynamical measurements; the total intensity is focused into a fiber-coupled spectrometer (SP).

IV. THE VCSOA UNDER THE INJECTION OF AN EXTERNAL FIELD

In this section, we study the optical response of the resonator to an injection beam when the VCSOA is operated above transparency. Transparency is a transition at which the dispersive nonlinearity vanishes and above which it becomes positive (focusing). Amplification also emerges at that point, and these two properties contribute strongly to the stability of CSs. Small signal amplification measurements have been performed on the VCSOA and have shown that amplification is present within the spectral range of cavity resonance for a pump intensity exceeding 18 kW/cm^2. The pump intensity at transparency cannot be measured precisely but can be estimated to be around 10 kW/cm^2 if derived from the measurement of the laser threshold and from the cavity parameters. Actually, we never observed patterns below this value.

We first scan the cavity detuning of the injected beam with respect to the cavity resonance ($\lambda_0 \sim 891.2$ nm). We pump the VCSOA over a 120 μm diameter spot with an optical intensity of 38 kW cm^{-2} and set the HB power to 50 mW and wavelength close to the cavity resonance. The near-field image sequence is presented with an inverted contrast on Fig. 2. In Fig. 2(a), the dark and larger area observed is the amplified spontaneous emission produced in the pumped region which gives the spatial scale of the patterns. The pattern at the center forms spontaneously when the wavelength of the injected beam is slightly blue detuned from the cavity resonance, as observed in [24]. As the injection wavelength is increasingly blue detuned from the cavity resonance, we observe that the patterns progressively spread over the whole pumped region [Fig. 2(b)–2(e)]. In fact, the pump generates heat and produces a radial thermal gradient [22] which has its counterpart in a cavity resonance gradient whose sign is such that the blue detuning is maximum at the center and decreases toward the periphery. Therefore, along a radius, the most peripheral regions reach the modulational instability threshold at a wavelength shorter than the central region, leading to the progressive spreading of the pattern with decreasing wavelength, over the whole pumped region. The strength of this gradient can be evaluated from Figs. 2(b) and 2(c) to 1.8 T Hz/100 μm, much larger than the gradient induced by the thickness inhomogeneity. The thermal gradient, however, cannot be reduced to the sole detuning since it has much more complex intertwined effects deriving from the shift of the band gap, which directly affects the α factor.

For large patterns, as shown in Fig. 2(f) in an enlargement of the central region, a breaking of the circular symmetry, imposed by the boundary conditions of the modulation insta-

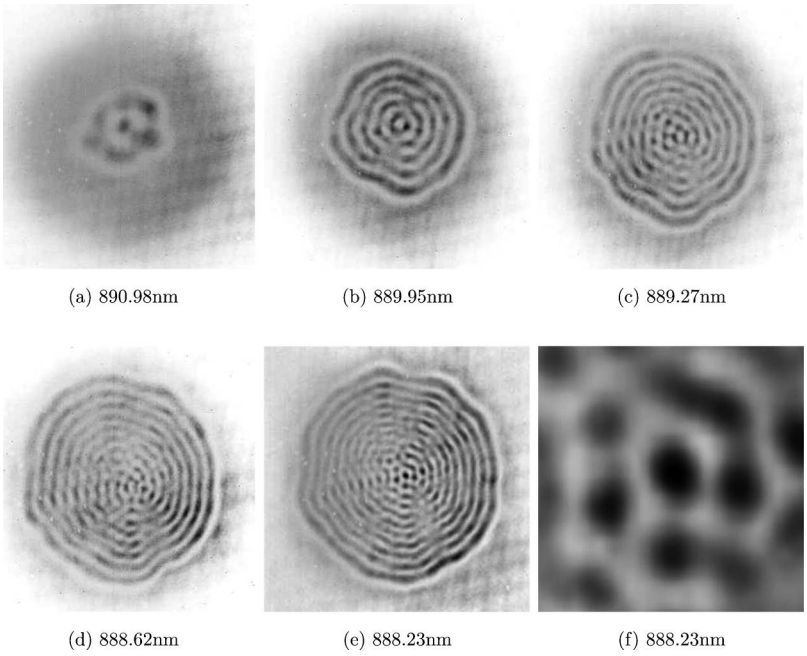

FIG. 2. Inverted contrast, near-field images of the intensity profiles of the output of the VCSOA under injection. The pump intensity is 38 kW cm^{-2}. (a), (b), (c), (d), and (e) images of the patterns for decreasing λ_{HB}. (f) Enlargement of the central region of pattern (e).

bility, is attained at the benefit of a hexagonal symmetry; the boundaries are far enough for the central part to become effectless. As one inspects the image closer to the periphery, rolls predicted by theory [6] on an infinite system adapt into concentric circles imposed by the conjunction of the radial thermal gradient and the symmetry of revolution of the pump beam.

We analyzed the periodicity of the patterns over a 80 μm diameter region by a 2D Fourier transform of the near-field images taken at different cavity detunings. We obtained thereby the characteristics of the transverse wave vector of the pattern. Figure 3 shows the dependance of the transverse wave vector square modulus q^2 of the pattern on the detuning of the HB wavelength λ_{HB} from resonance. The theoretical dependance established in [25],

$$q^2 = 8\pi^2 n_0^2(\lambda_0 - \lambda_{HB})/\lambda_0^3, \tag{1}$$

fits very well with the experimental points, using the parameters λ_0=884.04 nm and n_0=3.3, which is a signature of the nonlinear origin of the patterns. Moreover, the value of the refractive index that enters the linear fit witnesses the large nonlinear index change ($\Delta n \sim -0.3$) induced by the high carrier density injected by the pump beam. Note that despite the observance, in average, of the expected law, one can observe along a radius, for a given pump level, a slight but measurable inward decrease of the spatial period as a consequence of the induced thermal gradient. As the thermal dependance of the system affects not only the detuning parameter but others such as the Henry factor or the gain factor, an analysis of the radial dependance of the spatial periodicity could not be undertaken in the scope of this article.

We proceeded to a second experiment were we scanned the pump intensity, keeping λ_{HB} constant at the same intensity as in the previous experiment. In Fig. 4 we present the succession of patterns observed when increasing the pump intensity from 12 kW/cm^2 to 22 kW/cm^2 at a fixed HB wavelength (λ_{HB}=888.21 nm) over a 120 μm spot diameter. At low pump intensity, we observe a single localized structure [Fig. 4(a)], then a second spot appears [Fig. 4(b)], and the system progressively evolves to an extending pattern with a decreasing spatial period. Our analysis is similar to that of the first experiment concerning the radial gradient induced by heat except that in this configuration, due to the excitation conditions, the injection wavelength is constant but the cavity resonance moves to the red with the pump intensity. Then the system has to face two counteracting contributions to the resonance shift: a blue shift due to the carrier induced index reduction and a thermally induced red shift. Contrary to what was reported in [26] with relatively small area VCSEL, the thermal contribution in this experiment seems to overcome the carrier induced one and lead to an overall red shift of the resonance wavelength of the cav-

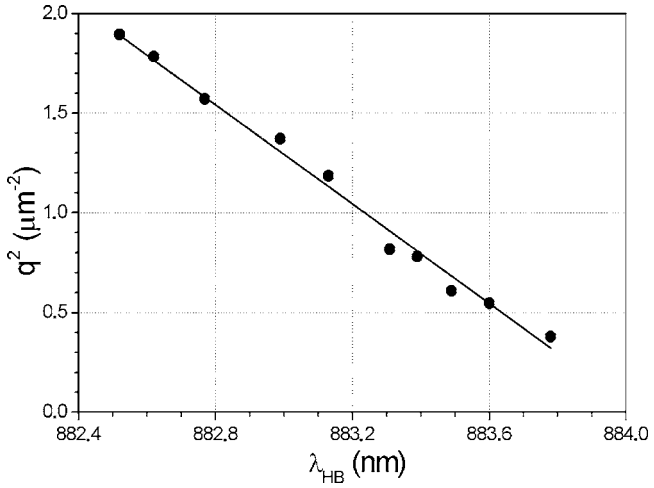

FIG. 3. Theoretical dependance (line) of the squared transverse wave vector of the patterns with the HB wavelength vs that measured (dots) on patterns with a 80 μm pump diameter.

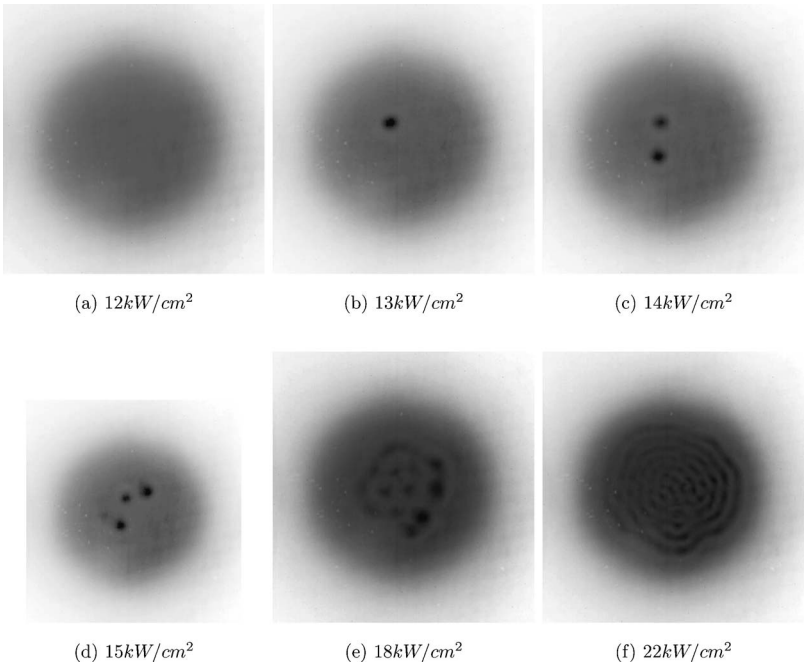

FIG. 4. Inverted contrast, near-field images of the output intensity of the VCSOA for a fixed HB wavelength $\lambda_{HB}=888.21$ nm and for various pump intensities on a 120 μm diameter.

ity. The detuning is therefore increasingly negative, and we note an increase of the region concerned by the patterns, i.e., above the modulation instability threshold, together with an increase of the pattern wave vector modulus.

V. COHERENT AND INCOHERENT WRITING AND ERASURE OF A CS

Switching is a key property of CS, and the switch duration determines the speed at which CS-based devices can be addressed. We demonstrate that under properly chosen parameters, CS may be written and erased by injecting a WB as a local perturbation. As was first shown in [18], the possibility to use a WB, either coherently or incoherently with respect to the HB, is analyzed in detail here.

In a first experiment, we ramped the HB power and monitored the local intensity at the CS. Bistability was observed between the homogeneous background and the localized structure. Then we optically biased the system close to the center of the local bistability cycle. The pumped diameter was set to 80 μm. The WB was extracted from the HB by PBS1. A half-wave plate controlled the power balance between the two ports of PBS1. We set the WB power on the sample to about 10 mW. In order to change the phase Φ of the WB relative to that of the HB, mirror M1 could be moved by the piezoelectric holder (PZT) on which it was mounted. On the sample, the waist of the WB was about 10 μm, which is comparable to the characteristic diameter of a CS. In this case, for a WB in phase with the HB ($\Phi=0$ rad), the CS is switched on, and it could be switched off by injecting the WB again with $\Phi=\pi$. In order to carry out a complete on-off CS switching sequence, we inserted an electro-optic modulator (EOM) on the WB path to deliver 100 ns width pulses. The power output was detected by the APD with 90 ps rise time over a 20 μm spot wise, at the same transverse location where the WB addressed the CS. The detected signal was analyzed by a 3 GHz analog bandwidth oscilloscope (Tecktronix 694C). By ramping the PZT and appropriately triggering the WB in order to obtain a first $\Phi=0$ pulse followed by a $\Phi=p\pi$ pulse where p is odd, we could realize a sequence where a CS switched ON and OFF repeatedly (Fig. 5) in a controlled manner. Unfortunately, the various electromechanical instabilities in the system to which Φ is particularly sensitive revealed a complete study of the writing and erasure process to be impossible. These instabilities are also responsible for the millisecond-scale jitter between the WB application and the system response. This is observable in the instants when the CS is written and erased (Fig. 5).

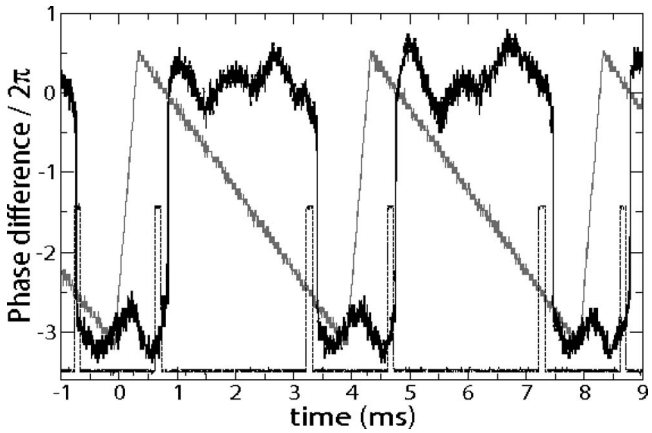

FIG. 5. Triggered coherent CS switch on and off by modulating the relative phase Φ in such a manner to obtain a 100 ns pulse width WB successively, in or out of phase with the HB ($\lambda=883.09$ nm). Dark line: local intensity at the CS location, dashed line: 100 ns pulse trigger (rising edge), and gray line: ramp to the PZT controlling the phase difference (left axis) ($I_P=39$ kW/cm^2).

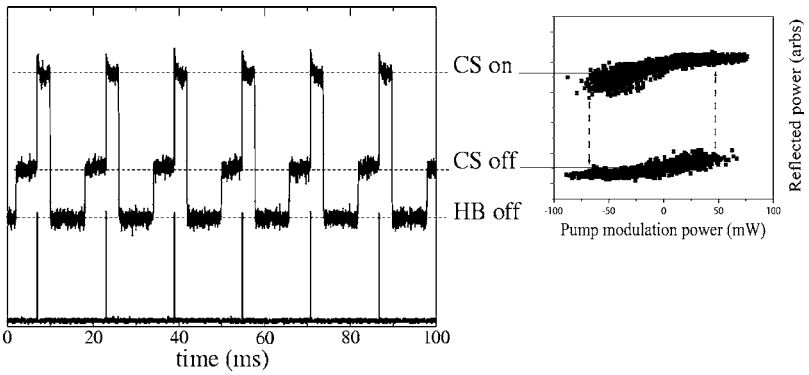

FIG. 6. Triggered incoherent switch on of a CS after local excitation with a 60 ps writing pulse. (Left) Upper trace: local intensity at the CS. A mechanical shutter erases the CS by shutting down the HB after each writing pulse. Lower trace: Writing pulse trigger launching a single 60 ps pulse. (Right) Reference hysteresis cycle of reflected vs PB powers.

The possibility to excite a CS with an incoherent beam can appear very interesting since it releaves the system from the relative phase dependence between the HB and the WB and from the quite sensitive dependence of the HB on the wavelength detuning from the cavity resonance. Therefore, in a second experiment we replaced the coherent WB by a beam produced by a pulsed Ti:Sa laser (TiSa2), whose wavelength is different from that of the HB or the pump beam. The acousto-optic modulator (AOM) allows one to select a single 60 ps writing pulse. The WB operates at around 795 nm in the pumping window where the absorption in the active layer is high. We used BS3 on the pump beam path to inject this perturbation in the system in the form of a 10 μm size spot. We used the same detection setup as in the previous experiment. We checked for the local bistability of the localized structure by varying the pump beam slightly around a constant bias. We recorded a hysteresis cycle [Fig. 6(a)] showing on and off switching of the CS controlled by the global optical pump. At first, with an incoherent beam, it seems only possible to write a CS because with such a beam one can only add carriers locally, contrary to what occurs with a coherent beam that can add to or subtract from the HB. Therefore, we did not expect writing to be followed by an erasing procedure with the same approach. This is why we modulated the HB with a mechanical shutter at a frequency around 50 Hz. When the HB was on, we triggered the WB to write a CS. Indeed, the bistable character of the CS ensured that once it was switched on, it persisted even when the WB was gated off. Erasure was obtained by crudely gating off the HB and resetting the system back to its low intensity homogeneous level. The two gates were delayed by 5 ms, long enough for the system to reach the stationary state before we applied the WB. We showed [Fig. 6(b)] that a triggered CS switch on was possible exactly as in the coherent excitation case. The minimum average power required was of the order of 1 mW.

The dynamical observations in the incoherent context showed that the CS switch on process is comparable to the regular CS switching process in a semiconductor microcavity with a coherent WB [10,15–19]. However, in this type of excitation, the writing pulse creates carriers at high energy that cascade very rapidly to the bottom of the bands. By contrast with a coherent excitation, writing is initiated by the local excess of carriers. This process was characterized, just after the application of the WB, as being the sum of the lethargic time (delay time) during which the intensity does not grow significantly and of the buildup time of CS intensity (rise time). The second one is very fast, of the order of 1 ns, and is ruled by the carrier lifetime [Fig. 7(b)]. The 200 ns delay in the switch-on time can either be attributed to a local thermal effect or have a dynamical origin. A detailed analysis would have required a stabilization of the temperature to better than 10^{-2} K, not currently available in our experiment.

It was rather surprising that CS erasure could also be obtained by setting the pump bias away from the center of the local hysteresis, closer to the switch off turning point, and sending a single pulse. A typical incoherent erasure process is shown in Fig. 7(b). The mechanisms of incoherent erasure are still not completely elucidated, but there are strong indications that fast radiative recombination can be invoked. This is one of the most probable mechanisms that could be responsible for a sudden decrease of light emission under carrier population effects. However, the repetition of subsequent writing and erasure of CS by application of weak and strong WB pulses could not be attained. The explanation lies in the fact that each of the writing and erasure processes require a different bias point with respect to the hysteresis cycle, which in the present sample prevents the sequence of such events.

In this section, we have demonstrated experimentally the possibility to repeatedly write and erase CSs with coherent perturbations and repeatedly write with incoherent perturbations. Moreover, incoherent erasure was also demonstrated. These two mechanisms are quite complementary in the sense that they address the CS through either of the two intricated components: the field (coherent part) and the carriers (incoherent part). Finally, the dissymmetry between the incoherent

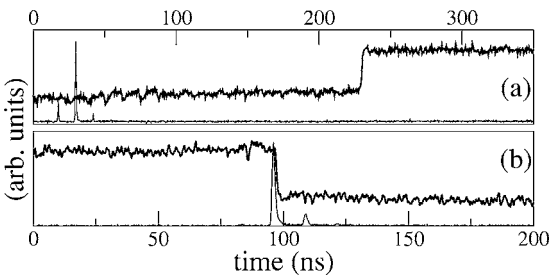

FIG. 7. CS incoherent switch on and off dynamics triggered by a 60 ps pulse (λ=876.95 nm, I_P=26 kW/cm^2). Thick line: Local intensity at the CS. Thin line: Writing/erasure pulse. (a) Writing of a CS. (b) Erasure of a CS.

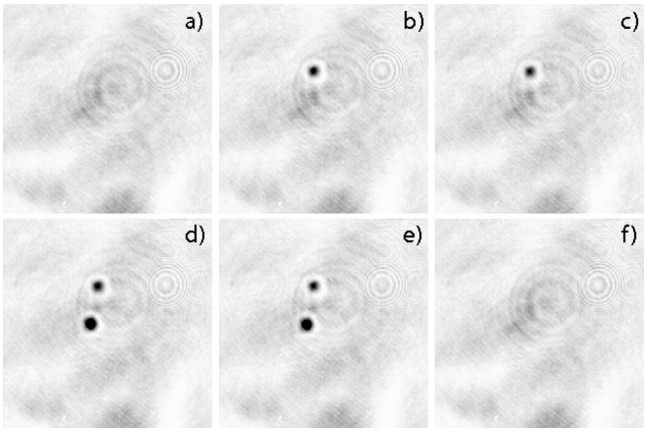

FIG. 8. Inverted contrast and intensity distribution of the output field (λ_{HB}=877.42 nm). (a) The holding beam is on and the WB is blocked. (b) A 10 μm incoherent focused WB (P_{WB}=53 mW) targets a point into the homogenous region; it induces the creation of one CS. (c) The WB is blocked again and the CS remains. (d) The WB is displaced and switched on again to generate a second CS. (e) We blocked the WB and the two CS coexist. (f) After the switch off of the HB we come back to the initial situation (a) by restoring the HB.

writing and erasure times needs to be investigated more thoroughly in order to better understand their mechanisms.

VI. CS CONTROL

One of the main properties of CS resides in the existence of a regime of mutual independence of two CSs. The possibility of controlling two CSs in an independent way using a coherent writing beam has been shown in [7,15]. This demonstration was also possible in our system, but we focused on the possibility of carrying it out using an incoherent WB. In this section we show the influence of impurities and the possibility to obtain up to five CSs.

In order to realize the CS control sequence with an incoherent WB, we fixed all parameters to values such that two solitons display hysteresis cycles with overlapping PB power range. Starting with no spot, we injected the incoherent WB at a first location where a CS was generated. We then, repeated the same operation at a different location to generate a second CS. As explained in the previous section, switch on and off of a CS with an incoherent WB cannot occur in the same parameter range. Thus, switch-off for these two CSs was obtained by removing the HB for a few milliseconds, which finally cycled the system back to the homogeneous situation. The full series, showing the successive incoherent writing of two independent CSs, is displayed in Fig. 8.

Theory explains the trapping role of sample roughness and impurities [8,15]. In our case, the thermal gradient forces the presence of CSs in the center of the pumping region. When we chose a region on the sample where the number and the strength of impurities were high enough to compensate for the thermal gradient, we were able to obtain five cavity solitons (Fig. 9).

The positions of these CSs are determined by those of the strongest impurities. In this case, CSs were spontaneously created by increasing the PB power. Indeed, we knew that CSs may be switched on by a WB as well as they could be induced by the noise present in the system. Moreover, it was not possible to control all five CSs within the same range of parameters. This was due to the fact that they did not appear spontaneously for the same PB power. When we increased the PB power, those that appeared previously were expelled from the bistable range within which they are controllable.

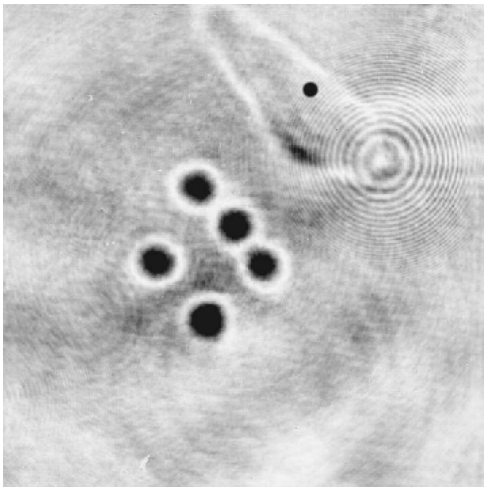

FIG. 9. Inverted contrast intensity distribution of the output field showing the presence of five CSs.

In a different experiment, we showed the ability to control a CS in the presence of three others [Fig. 10(c)]. Up to four CSs were obtained as we increased the PB power. After the first one appeared, the second one did for a slightly higher

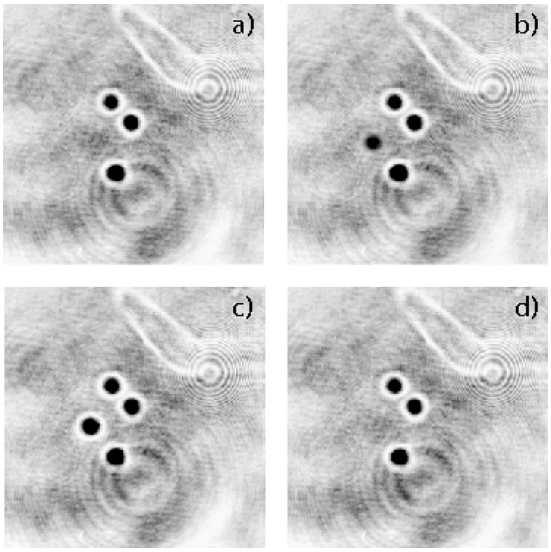

FIG. 10. Inverted contrast and intensity distribution of the output field. (a) The HB is on and the WB is blocked (the presence of three CSs). (b) A 10 μm incoherent focused writing beam (P_{WB}=53 mW) targets a point into the homogenous region. (c) It induces the creation of a fourth CS; the WB is blocked again and the fourth CS remains. (d) After having switched off the HB, we come back to the initial situation (a) with the three CSs by restoring the HB.

PB power. This difference was sufficiently small to allow the simultaneous control of these two CSs as in Fig. 8. The third CSs, though, appeared for a PB power even higher, for which value the two first CSs were not controllable anymore. Finally, a fourth CS appeared for a PB power which again made the third CS lose its controllability, but when we drove them back within their bistability range, they showed all the characteristics of a CS and in particular, the possibility to be controlled using a WB. We started on with three CSs [Fig. 10(a)] spontaneously created by increasing the HB. Then we addressed the incoherent writing beam [Fig. 10(b)] and created a CS that persisted after we removed the WB [Fig. 10(c)]. Finally, after switching off the holding beam during a few milliseconds, we came back to the initial situation [Fig. 10(d)]. This demonstrated the writeability and erasability of a CS in the presence of other neighboring CSs.

In this section we have shown the possibility to control (switch on and off) a cavity soliton using a incoherent WB. We also showed the possibility to obtain the simultaneous coexistence of five CSs. However, the simultaneous control of these five CSs requires a reduction of the various sources of inhomogeneities in the system and in particular, reduction of the thermal gradient.

VII. CONCLUSION

In this article, we have shown the possibility to obtain and control cavity solitons in optically pumped semiconductor microresonators thanks to an original cavity design optimized to improve the uniformity of the pumped region and to further reduce the heat produced by the optical pumping. These improvements have been able to produce, in particular, the coherent and incoherent on and off switching of cavity solitons. The complementarity of these two mechanisms are of double interest. From the conceptual viewpoint, each brings emphasis on a particular facet of the two physical parameters of importance in transverse nonlinear optics in semiconductor cavities, namely, the electromagnetic field and the excitation density, and demonstrate that each can be used as an external control parameter. From a prospective viewpoint, new strategies can be considered for optical information processing with cavity solitons by the additional possibility to use writing beams free of phase control. This mechanism also introduces the convenience of realizing wavelength conversion. We have also demonstrated the coexistence of up to five cavity solitons, even though their simultaneous control was not yet achieved. This is a first step in the use of sets of independently controlled cavity solitons. Actual achievement requires the reduction of inhomogeneities and thermal gradients in the system. This can be expected by the increase of the transverse size, rejecting sources of nonuniformities at the periphery of the system.

ACKNOWLEDGMENTS

This work has been partially supported by the European Union through the FunFACS Project and by the Region Ile de France.

[1] A. J. Scroggie, J. Jeffers, G. McCartney, and G. L. Oppo, Phys. Rev. E **71**, 046602 (2005).
[2] B. Schapers, M. Feldmann, T. Ackemann, and W. Lange, Phys. Rev. Lett. **85**, 748 (2000).
[3] M. Saffman, D. Montgomery, and D. Anderson, Opt. Lett. **19**, 518 (1994).
[4] P. Ramazza, S. Ducci, S. Boccaletti, and F. Arecchi, J. Opt. B: Quantum Semiclassical Opt. **2**, 399 (2000).
[5] R. Neubecker, G. L. Oppo, B. Thuering, and T. Tschudi, Phys. Rev. A **52**, 791 (1995).
[6] M. Brambilla, L. A. Lugiato, F. Prati, L. Spinelli, and W. J. Firth, Phys. Rev. Lett. **79**, 2042 (1997).
[7] S. Barland, J. Tredicce, M. Brambilla, L. Lugiato, S. Balle, M. Giudici, T. Maggipinto, L. Spinelli, G. Tissoni, T. Knoedel *et al.*, Nature (London) **419**, 699 (2002).
[8] R. Kuszelewicz, I. Ganne, I. Sagnes, G. Slekys, and M. Brambilla, Phys. Rev. Lett. **84**, 6006 (2000).
[9] V. B. Taranenko, I. Ganne, R.J. Kuszelewicz, and C. O. Weiss, Phys. Rev. A **61**, 063818 (2000).
[10] I. Ganne, G. Slekys, I. Sagnes, and R. Kuszelewicz, Phys. Rev. E **66**, 066613 (2002).
[11] S. Barbay, J. Koehler, R. Kuszelewicz, T. Maggipinto, I. Perrini, and M. Brambilla, IEEE J. Quantum Electron. **39**, 245 (2003).
[12] I. M. Perrini, S. Barbay, T. Maggipinto, M. Brambilla, and R. Kuszelewicz, Appl. Phys. B **81**, 905 (2005).
[13] S. Barbay, Y. Ménesguen, I. Sagnes, and R. Kuszelewicz, Appl. Phys. Lett. **86**, 151119 (2005).
[14] P. Coullet and C. Toniolo, Chaos **14**, 839 (2004).
[15] X. Hachair, S. Barland, L. Furfaro, M. Giudici, S. Balle, J. R. Tredicce, M. Brambilla, T. Maggipinto, I. M. Perrini, G. Tissoni, and L. Lugiato, Phys. Rev. A **69**, 043817 (2004).
[16] X. Hachair, L. Furfaro, J. Javaloyes, M. Giudici, S. Balle, J. Tredicce, G. Tissoni, L. A. Lugiato, M. Brambilla, and T. Maggipinto, Phys. Rev. A **72**, 013815 (2005).
[17] D. Michaelis, U. Peschel, and F. Lederer, Opt. Lett. **23**, 337 (1998).
[18] S. Barbay, Y. Ménesguen, X. Hachair, L. Leroy, I. Sagnes, and R. Kuszelewicz, Opt. Lett. **31**, 1504 (2006).
[19] V. Taranenko and C. Weiss, Appl. Phys. B: Lasers Opt. **72**, 893 (2001).
[20] V. Taranenko, C. Weiss, and W. Stolz, Opt. Lett. **26**, 1574 (2001).
[21] M. Grabherr, R. Jaeger, M. Miller, C. Thalmaier, J. Heerlein, R. Michalzik, and K. Ebeling, IEEE Photon. Technol. Lett. **10**, 1061 (1998).
[22] Y. Ménesguen and R. Kuszelewicz, IEEE J. Quantum Electron. **41**, 901 (2005).
[23] W. J. Firth and A. J. Scroggie, Phys. Rev. Lett. **76**, 1623 (1996).
[24] T. Ackemann, S. Barland, J. R. Tredicce, M. Cara, S. Balle, R. Jaeger, M. Grabherr, M. Miller, and K. J. Ebeling, Opt. Lett. **25**, 814 (2000).
[25] W. Firth and A. Scroggie, Europhys. Lett. **26**, 521 (1994).
[26] S. Hegarty, G. Huyet, P. Porta, J. McInerney, K. Choquette, K. Geib, and H. Hou, J. Opt. Soc. Am. B **16**, 2060 (1999).